Surface & Coatings Technology 206 (2012) 4645–4650

Contents lists available at SciVerse ScienceDirect

Surface & Coatings Technology

journal homepage: www.elsevier.com/locate/surfcoat

Nanomechanical and electrochemical properties of ZrN coated NiTi shape memory alloy

Daiane Roman [a], Juliane C. Bernardi [a], Carla D. Boeira [a], Fernando S. de Souza [b], Almir Spinelli [b], Carlos A. Figueroa [a], Rodrigo L.O. Basso [a,c,*]

[a] Centro de Ciências Exatas e Tecnologia, Universidade de Caxias do Sul, Caxias do Sul, RS, 95070-560, Brazil
[b] Departamento de Química, Universidade Federal de Santa Catarina, Florianópolis, SC, 88040-900, Brazil
[c] Universidade Federal da Integração Latino Americana, Foz do Iguaçu, PR, 85867-970, Brazil

ARTICLE INFO

Article history:
Received 17 December 2011
Accepted in revised form 11 May 2012
Available online 19 May 2012

Keywords:
Nitinol
Zirconium nitride
Crystallographic texture
Nanomechanical properties
Electrochemical properties

ABSTRACT

Zirconium nitride (ZrN) thin films were deposited on NiTi and Si substrates in the 23–570 °C temperature range by direct current reactive magnetron sputtering using N_2/Ar gas mixture. The film hardness, corrosion behavior, phase composition, and texture were determined. The deposited films were composed mainly by the cubic ZrN phase, whose texture varies with substrate temperature, changing progressively from (111) to (200) texture as the temperature increases. The hardness of the films is influenced by the texture and has a linear relationship with the ratio of the texture coefficients P(111)/P(200). The higher hardness is obtained for ZrN thin films with (200) texture. Electrochemical tests show that NiTi coated with (200)-oriented ZrN films has higher tendency to passivation and greater stability of the passive film as compared to (111)-oriented ZrN films, despite no abrupt changes was observed when the texture changes from (111) to (200).

1. Introduction

Thin film coatings and plasma treatment are well known to improve the mechanical, chemical and magnetic properties of steels and tools [1–3]. Zirconium nitride (ZrN) is a transition metal (TM) nitride, similar to titanium nitride (TiN), applied to improve the surface properties. Its physical characteristics resulting from both metallic and covalent bonds can combine good electrical and thermal conductivity with high hardness, high melting temperature and chemical inertness. Thin films composed of binary nitrides can present a well-known NaCl type crystalline structure and, like TiN have mechanical properties depending on the crystallographic texture of the deposited film [4]. In all the applications, the lifetime and performance of the coatings are influenced by the control of the microstructure and texture. Despite all the research efforts, the physical mechanisms concerning the evolution of texture and grain growth of the films are not completely clarified. In particular, the texture in polycrystalline TiN and ZrN thin films has different explanations in many published works. Some authors proposed that the texture evolution is governed by the strain energy minimization during the growing process [5–8]. On the other hand, several authors report that the texture is related with the adatom mobility and the kinetic-driven mechanisms [9–12]. Other authors found that both the strain energy and the surface energy act in a competition mode during the grain growth. Also, it was suggested for TiN thin films that in the initial stage of growth, the (002) planes were aligned to the substrate surface axis to minimize the surface energy. Furthermore, at later stages, the (002) growth front tilted away from the surface by about 60° to relax the strain, causing the change of the preferred growth direction favoring the (111) planes [13]. Therefore, the explanation of the leading process for the texture of TM nitride thin films remains an issue to be addressed. Besides the mechanical properties that are related with crystallographic texture, the chemical inertness of thin films would also be related with this feature. The chemical inertness in aggressive media is a mandatory feature for biocompatibility of TM nitride thin films. In particular, ZrN thin films have the potential to be used as coating for biomaterials and for bioelectronic devices, due to its biocompatibility together with good electrical, thermal and mechanical properties [14,15]. Generally, the choice for a biomaterial is made by taking into account its corrosion resistance. However, even with the corrosion protection feature of such materials, the dissolution process that occurs in aggressive media containing chlorine ions can lead to the contamination of the organism with metal ions, affecting the biocompatibility and mechanical properties of a prosthesis [16]. As a consequence, in such applications, as in biomedical implants, severe restrictions are imposed on the materials to be used concerning stability in aqueous solutions with high concentrations of electrolytes. For these reasons, it is mandatory to understand the corrosion behavior of the

* Corresponding author at: Centro de Ciências Exatas e Tecnologia, Universidade de Caxias do Sul, Caxias do Sul, RS, 95070-560, Brazil. Tel./fax: +55 54 3218 2764.
E-mail address: rlobasso@ucs.br (R.L.O. Basso).

0257-8972 © 2012 Elsevier B.V. Open access under the Elsevier OA license.
doi:10.1016/j.surfcoat.2012.05.039

ZrN thin films on different substrates used as biomaterials and to correlate the chemical inertness with the texture and with the deposition parameters to obtain high corrosion protection maintaining the mechanical resistance. The aim of the present work is to investigate the corrosion resistance and hardness of ZrN thin films deposited at different temperatures on NiTi, C and on Si substrates. We focused in the microstructure in relation with the corrosion and mechanical properties.

2. Experimental

In order to prepare and characterize the ZrN films, which involves the preparation of the samples for X-ray diffraction analysis (XRD) and electrochemical tests, we choose Si(100) wafer and NiTi as substrates, respectively. The NiTi samples were grounded after being cut and then polished with an alumina suspension up to 0.1 μm of particle size. The samples were then cleaned with acetone in an ultrasonic bath for 30 min. The ZrN thin films were deposited using direct current reactive magnetron sputtering, applying a power of 100 W on a Zr target in Ar/N_2 atmosphere. It was used floating potential bias during deposition and the current density was 0.60 mA/cm^2. The base pressure in the chamber was 10^{-7} mbar. The substrate temperature was varied from 25 to 570 °C maintaining a total pressure of 2×10^{-2} mbar with a flux of 5.0 sccm for Ar and 0.88 sccm for N_2. After the deposition, the samples were slowly cooled in vacuum inside the deposition chamber. In order to study the corrosion behavior of the ZrN coated-NiTi samples, open-circuit potential (OCP) measurements and potentiodynamic polarization tests were performed in a VoltaLab PGZ100 potentiostat/galvanostat. The electrochemical tests were carried out at 37 °C in non-deaerated solutions. The electrolyte was an artificial saliva solution AFNOR S90-701 prepared using analytical grade reagents without previous purification. ZrN-coated- or uncoated-NiTi substrate of circular geometry was employed as the working electrode. For the corrosion tests, the thin film area to be studied was defined by partially covering the sample with an insulating resin. A 0.95 cm^2 area of the sample was exposed to the electrolytic solution. Before each experiment the working electrode was degreased with acetone, cleaned with ethanol, and rinsed with distilled and deionized water. A graphite rod was used as auxiliary electrode and a saturated calomel electrode (SCE) was the reference connected to the cell by a salt bridge and a Luggin-Haber capillary. All potentials mentioned in the text are quoted versus this reference electrode. Potentiodynamic polarization curves were obtained at 1 mV s^{-1} scan rate, after 60 min recording the open-circuit potential (OCP). The potentiodynamic polarization started at the value of 250 mV more negative than the OCP and followed to the positive direction of potentials. The breakdown potential-E_b (the potential where the passivating film begins to break down) was taken as the value at which the current density sharply increases during the positive potential scan. The hardness and reduced elastic modulus measurements were accessed by nanoindentation tests using a NanoTest-600 equipment manufactured by Micro Materials Ltd., equipped with a three-sided pyramidal diamond tip (Berkovich indenter). The unloading portion of load–depth curves was analyzed, allowing estimating values for film hardness [17]. Nanoindentation tests were performed at a load rate of 0.01 mN.s^{-1} and a constant indentation depth of 20 nm. The substrate effect on hardness measurements appears when the indentation depth reaches between 10% and 20% of the total thickness. In order to avoid this effect, we chose the lower limit (10%) to perform our measurements. The elastic modulus was calculated by using a Poisson ratio of 0.16 for ZrN [18]. The crystalline structure of the ZrN films was studied by X-ray diffraction at room temperature with a grazing incidence of 0.6° on an X-ray diffractometer (Shimadzu XRD-6000) with Cu-Kα (λ = 1.54064 Å) radiation (U = 40 kV and I = 30 mA), using as reference XRD data files from ICSD (Inorganic Crystal Structure Database) [19]. On the study of the thickness and the microstructure, scanning electron microscopy (SEM) analysis was used on the cross-section of the samples with a Shimadzu SSX-550 electron microscope. The thickness of the thin films was directly measured from the SEM images.

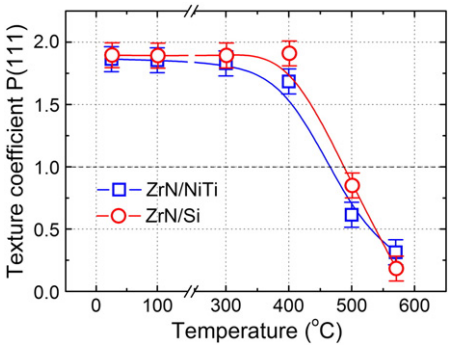

Fig. 2. Texture coefficient P(111) obtained by Harris method for ZrN thin films deposited at different temperatures on NiTi and on Si substrates. The dashed line at P(111) = 1.0 represents the situation where no texture is present. For values below 1.0, the texture is on (200) direction.

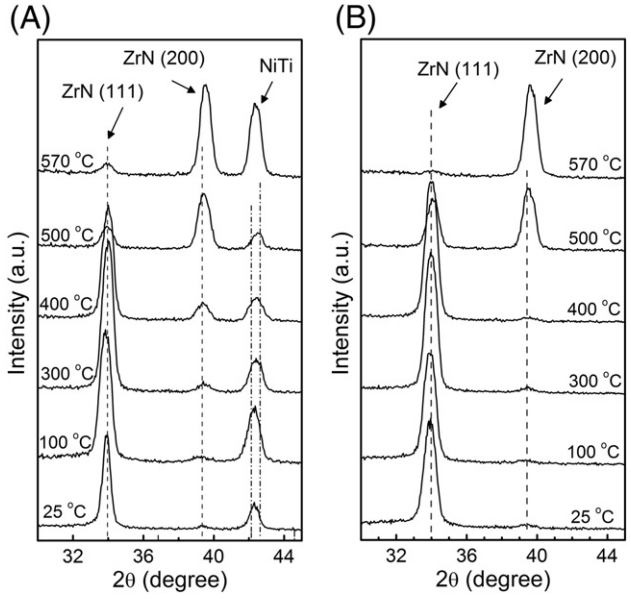

Fig. 1. XRD patterns for ZrN thin films deposited at different temperatures (A) on NiTi substrate and (B) on Si substrates.

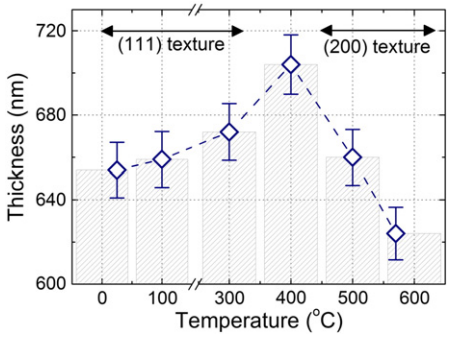

Fig. 3. Thickness of ZrN thin films deposited on NiTi substrates as measured by SEM analysis. The thin films were deposited at different temperatures.

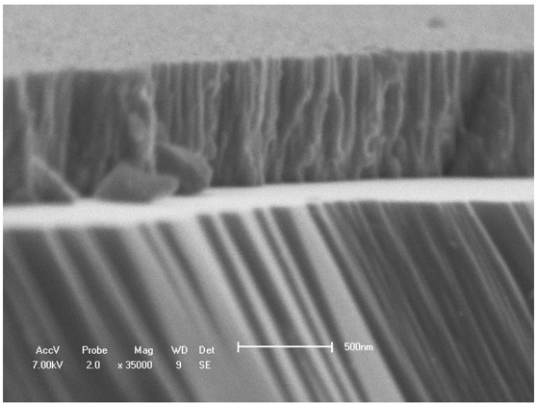

Fig. 4. Cross-section SEM image for ZrN thin film deposited on silicon substrate over 1 h at 500 °C.

3. Results

3.1. XRD results

Fig. 1A shows the XRD patterns for ZrN/NiTi samples prepared with different deposition temperatures. The figure shows the Bragg peaks associated to the ZrN phase (ICSD — 167851) and also due to the NiTi substrate (ICSD — 646967) [19]. The two most intense reflection planes are (111) and (200) for the ZrN phase and these two peaks present a very interesting behavior. For temperatures up to 400 °C, the most relatively intense peak is the (111) at (34.0 2θ), and for temperatures above 400 °C, the (200) peaks at (39.4 2θ) is the most relatively intense. This behavior is clearly due to a texture on the ZrN films. For ZrN/Si samples, only the Bragg peaks associated to the ZrN phase were observed as shown in Fig. 1B. In order to study the texture evolution at different deposition temperatures, the texture coefficient $P(hkl)_i$, was calculated by the Harris method [20,21]. As revealed in Fig. 2, the ZrN thin films exhibited a relatively strong (111) texture [$P(111)>1$] for deposition temperatures from 25 °C up to 400 °C. For higher temperatures (500 and 570 °C) the texture coefficient is $P(111)<1$. This clearly reveals the change of the texture towards the (200) planes for deposition temperatures of 500 and 570 °C for ZrN thin films deposited on both Si and ZrN substrates. At 570 °C no plateau is reached indicating that the texture may evolve with higher temperature.

3.2. Film thickness and morphology

The thicknesses for the ZrN thin films deposited at different temperatures are shown Fig. 3. All the films were deposited for 1 h. The figure shows an apparent increasing on thickness for temperatures up to 400 °C and an apparent decreasing for higher temperatures. However, the difference between the thicknesses for all the samples is within 10% and we consider the thickness the same for all the samples.

The microstructure of the films was observed by SEM. Fig. 4 shows the cross-section SEM image for ZrN thin film deposited on silicon substrate over 1 h at 500 °C. The microstructure observed has columnar characteristics indicating the preferential direction of growth perpendicular to the surface plane of the substrate [22]. The surface microstructure was analyzed after the deposition processes (not shown) in order to verify the roughness and porosity. All the samples presented the same morphology indicating no influence of the texture on the porosity or on the roughness.

3.3. Hardness results

Fig. 5A shows the evolution of the hardness of ZrN thin films as a function of deposition temperature: a clear tendency is observed. On the one hand, the ZrN thin films deposited at temperatures lower than and including 300 °C, keep their hardness values around 15 GPa. On the other hand, the ZrN thin films deposited at temperatures higher than and including 500 °C keep their hardness values around 19 GPa. Therefore, we can divide the samples into two groups according to the hardness values. In between of both groups of hardnesses, the ZrN thin film deposited at 400 °C shows an intermediate hardness of 17 GPa. One can notice that the results were obtained for three different sets of samples with good reproducibility. This behavior may be associated with crystallinity and texture, both temperature-dependent properties, as will be discussed below.

Fig. 5B shows the variation of the H^3/E^2 ratio with the deposition temperature of ZrN thin films. As shown above for hardness behavior, there are also two groups with H^3/E^2 ratio constant with deposition temperature ($T \leq 300$ °C and $T \geq 500$ °C). However, a minimum H^3/E^2 ratio is observed at 400 °C, whereas the hardness reaches an intermediate value (Fig. 5A).

3.4. Electrochemical behavior

Fig. 6A shows the open-circuit potential curves corresponding to ZrN coated- or uncoated-NiTi alloy. It is easily observed that after

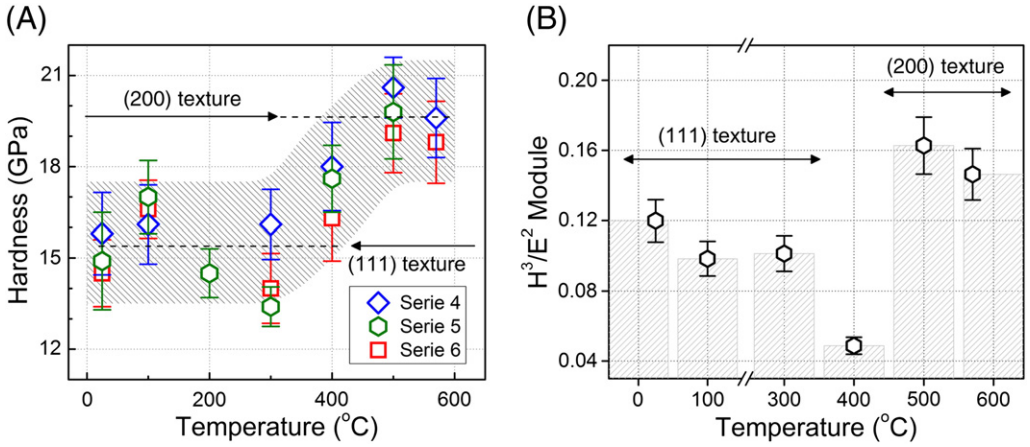

Fig. 5. (A) Surface hardness measured by nano-indentation tests at depths of 20 nm from the surface. The results were obtained for different sets of ZrN thin films deposited at different temperatures. There are two levels of hardness represented by the dashed lines. One around 15.5 GPa for samples presenting (111) texture and another one at 19.5 GPa for samples presenting (200) texture. (B) H^3/E^2 ratio for the different deposition temperatures used to obtain the ZrN thin films. A minimum H^3/E^2 ratio is observed at 400 °C.

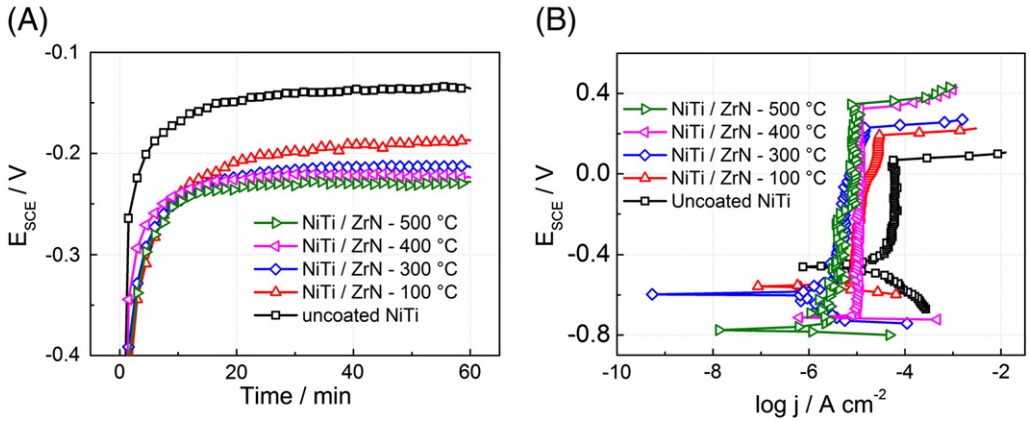

Fig. 6. (A) Open-circuit potential (OCP) measurements taken for 1 h. (B) Polarization curves for ZrN films deposited at different temperatures onto NiTi substrates. It was used as an artificial saliva solution (AFNOR S90-701) in order to study the corrosion behavior in a simulated biological fluid. The pristine NiTi sample was also measured and the result is showed by the black curve.

uncoated-NiTi alloy is immersed into electrolyte solution, the OCP-values rapidly increase in a few minutes, that characterizes the spontaneous formation of a passive layer at the electrode surface [23,24]. After around 15 min, the potential remains almost constant at −136 mV. For the ZrN coated-NiTi samples, the curves profile is the same, but the time for the stabilization of the potential is lower. As the deposition temperature increased the OCP-value shifted to negative values. For instance, the OCP-value for the ZrN film obtained at 500 °C is −228 mV. This indicates that ZrN coated-NiTi samples have higher tendency to spontaneous passivation than uncoated-NiTi alloy. This corrosion behavior has been attributed to the formation of a thin ZrN_xO_y and ZrO_2 layer on the top of the ZrN films when the samples were exposed to air [25]. Fig. 6B also points out for the influence of ZrN film and deposition temperature on the corrosion behavior of the studied material. The polarization curve for the uncoated-NiTi alloy is the characteristic of a material that is spontaneously passivated in the simulated body fluid solution used for the corrosion tests. As can be seen, the corrosion rate in the passive region is low ($<10^{-4}$ A cm^{-2}), the potential region over which the NiTi alloy remains passive is of 530 mV. This value was calculated as the difference between the breakdown potential-E_b (+70 mV) and the potential-E′ (-460 mV), determined at the beginning of the anodic polarization curve taking into consideration that the polarization curves do not show the ideal active–passive profile. For the ZrN coated-NiTi samples it was observed that E′ shifts to negative values as temperature deposition increases, likely OCP. It is also observed that the material is quickly passivated just after E′ is reached, so the material becomes to corrode more slowly. Hence, for all the ZrN coated-NiTi samples, the corrosion rate in the passive region decreased, the region over which the material remains passive increased and the breakdown potential shifted to more positive values as the deposition temperature increased. Table 1 summarizes the results obtained.

Table 1
Electrochemical parameters for ZrN films deposited at different temperatures onto NiTi substrates.

Temp./°C	OCP/mV	E′/mV	E_b/mV	(E_b − E′/mV)[a]
Uncoated NiTi	−136	−460	70	530
25 °C	−176	−484	93	577
100 °C	−187	−550	196	746
200 °C	−192	−556	214	770
300 °C	−213	−605	234	839
400 °C	−224	−713	328	1041
500 °C	−228	−774	352	1126

[a] Passive potential region.

4. Discussion

All the experimental results evidence a strong correlation with structural evolution of ZrN thin films. In particular, (200)-orientation seems to give the best response in terms of hardness and chemical stability. Thus, the texture evolution and interpretations about the formation of the (200)-orientation will be discussed below.

Several authors observed the texture (111) or (200) on TiN and ZrN thin films with NaCl-type structure and the texture of such structure was governed by the lowest overall total energy conditions, resulting from a critical competition between surface energy and strain energy [7,26,27]. Taking into account the texture and corrosion property relationship, some authors attributed the corrosion behavior to the texture and morphology of the surface. On the one hand, the texture affects the surface energy influencing the corrosion reactions. On the other hand, the surface morphology affects the surface area in contact with the corrosive media [28]. As observed by Park and Szpunar [29] when they studied the role of crystallographic texture and morphology on corrosion resistance of zinc based electrogalvanized coatings, they observed that (0001) plane has better resistance against corrosion attack than other planes, because the close packed plane has the lowest surface free energy. Comparing our results for electrochemical tests and for the texture development of the ZrN thin films, the best corrosion behavior was obtained for the (200)-oriented ZrN films. This result is in agreement with those observed by Park and Szpunar once the ZrN (200) planes also have the lowest surface free energy and better corrosion behavior. Also, the thickness of the films seems to play an important role on the texture. As pointed by Oh [7], the surface energy is dominant in the early stage of film growth, in which the (200) plane has the lowest surface energy and grows faster than other planes, resulting in the (200) crystallographic texture. Beyond a critical thickness, the strain energy begins to be dominant and the (111) texture is developed [7]. In a recent study [25] it was obtained by different film thicknesses for different deposition times, in agreement with those observed by Oh [7], where the strain energy is dominant beyond a critical thickness and the (111) texture is observed.

However, we believe that in our experiments the thickness does not dictate the texture evolution. This is due to the constant thickness (within 10% of variation) obtained for all the samples in the temperature range used (see Fig. 1), maintaining a roughly constant strain. Consequently, the substrate temperature seems to be the driven force governing the texture changes. Contrary of the explanation given by Oh and others, and based on stress analysis, Abadias concluded that the driven force governing the texture changes in TiN and in ZrN thin films was not due to the minimization of the strain

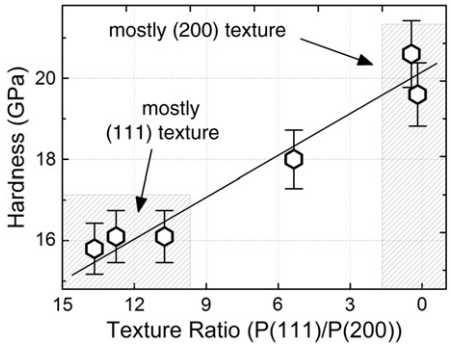

Fig. 7. Surface hardness obtained by nano-indentation tests at depths of 20 nm and its linear relationship with the ratio of the texture coefficients P(111)/P(200).

energy. It was proposed that kinetic effects are the main driving forces to textural development in TM nitrides deposited by MS and DIBS. Moreover, kinetic effects, in terms of diffusion, depend mainly on temperature.

In our results, the hardness evolution as a function of deposition temperature shows an interesting behavior which can be associated with the crystalline structure. Fig. 1 shows the XRD patterns of ZrN thin films as a function of temperature and Fig. 2 shows the texture dependence on deposition temperature. Indeed, the growth of the thin films of ZrN, is preferential along plane (111) or (200) at low or high deposition temperatures, respectively. Fig. 7 helps to understand that the hardness has a linear relationship with the ratio of the texture coefficients P(111)/P(200). Recently, this hardness anisotropy in TiN, depending on texture, was reported elsewhere [4]. Moreover, the same behavior was already observed in vanadium carbide thin films [30]. On the one hand, in (111) texture, zirconium atoms occupy tetrahedral interstitial sites which are in agreement to tetrahedral coordination when nitrogen atoms are considered as ligands or complex agents according to the crystal field theory [31]. On the other hand, in (200) texture, zirconium atoms occupy octahedral interstitial sites which are in agreement to octahedral coordination when nitrogen atoms are considered as ligands according to the same theory. Moreover, the ligand field stabilization energy for metallic centers in octahedral geometry is higher than in tetrahedral geometry [31].

Thus, zirconium atoms in octahedral coordination are more stable, energetically speaking, than in tetrahedral geometry. We believe that tetrahedral coordination is formed first at low temperature and, consequently, the texture along planes (111) could be though as a kinetic product. In addition, the increasing temperature produces a higher zirconium mobility and, consequently, the thermal energy allows zirconium atoms reaching the most stable configuration (octahedral coordination) transforming the texture along planes (111) at low temperatures in texture along planes (200) at high temperatures. As shown in Fig. 5A, the transition temperature can be assigned in about 400 °C where the hardness achieves intermediate values and significant contributions of both planes (111) and (200) are observed. Indeed, in these temperatures most of transition metals have enough mobility leading to diffuse towards the most stable configuration from a thermodynamic point of view [32]. A more stable system leads to increase the bond strength and, consequently, the hardness of the material which preferentially grows along orientation (200).

The elastic strain to failure (H^3/E^2) criterion, which has been proposed and consistently used to evaluate the resistance to plastic deformation of thin film coatings and to predict their resistance to wear [33] shows a minimum at about 400 °C where the transition between both textures takes place. According to the criterion, this minimum indicates a lower wear resistance due to plastic deformation. Strictly speaking, plastic deformation is an atomic mechanism which must involve permanent displacement of a group of atoms (cluster). In our material system, we have two types of cluster: (111)-oriented where Zr is located in tetrahedral coordination and (200)-oriented where Zr is located in octahedral coordination. We suggest that the transition between both textures allows the formation of intermediate atomic clusters which during indentation pressure from the tip (mechanical energy) are reorganized in the most stable arrangement (octahedral coordination) by plastic deformation. In such intermediate clusters, Zr atoms seem to be in the way of the most stable configuration in (200) orientation. Thus, the lowest H^3/E^2 should be measured at about 400 °C where a lower energy should be necessary to move Zr atoms from this intermediate position (transition state between (111) and (200)) to the final most stable configuration of octahedral coordination in (200) orientation.

Contrary to the hardness, the corrosion results in this work clearly show a monotonous increasing in corrosion resistance with increasing substrate temperature. Table 1 summarizes the corrosion parameters obtained and there is no evidence of texture influence on corrosion results once there is no abrupt changing in corrosion behavior when the texture changes from (111) to (200). Moreover, the SEM analysis of the surface prior the corrosion tests shows no significant differences on microstructure concerning roughness and porosity. Also, the influence of oxidation, favored by higher temperature during the deposition and after that (when samples were exposed to air), can play an important role in the corrosion resistance evolution. All these, indicates that, in our work, the main point in the corrosion behavior was the oxidation of the surface favored by the higher temperature during the deposition.

5. Conclusions

Hardness and corrosion behavior of ZrN thin films deposited at different substrate temperatures were evaluated and the results were related with the crystallographic texture development. For relative low deposition temperatures the (111) crystallographic texture was observed. On the other hand, at relative high deposition temperatures, (200) crystallographic texture was observed. The hardness of the films is influenced by the texture. The (200)-oriented ZrN films are harder than the (111)-oriented ZrN films, conferring higher mechanical resistance. Relatively high hardness was obtained with thin films showing (200) texture, and was only achieved for temperatures equal and above 500 °C. Also, hardness has a linear relationship with the ratio of the texture coefficients P(111)/P(200). The corrosion behavior was evaluated by potentiodynamic polarization experiments in artificial saliva. The results evidenced that ZrN coated-NiTi alloy has better performance toward corrosion than uncoated-NiTi. Also, (200)-oriented ZrN films have better performance toward corrosion than (111)-oriented ZrN films. Despite the changes in texture of the ZrN thin films, the corrosion resistance increased monotonous with increasing the substrate temperature.

Acknowledgments

The authors would like to acknowledge the MCT/CNPq and CAPES for the financial support. CLGA and JB receive grants from CAPES and DR, CAF, AS from CNPq. Special recognition goes to Israel Jacob Rabin Baumvol for his valuable comments and suggestions.

References

[1] M.V. Leite, C.A. Figueroa, S.C. Gallo, A.C. Rovani, R.L.O. Basso, P.R. Mei, I.J.R. Baumvol, A. Sinatora, Wear 269 (5–6) (2010) 466.
[2] R.L.O. Basso, C.A. Figueroa, L.F. Zagonel, H.O. Pastore, D. Wisnivesky, F. Alvarez, Plasma Process. Polym. 4 (S1) (2007) S728.
[3] R.L.O. Basso, V.L. Pimentel, S. Weber, G. Marcos, T. Czerwiec, I.J.R. Baumvol, C.A. Figueroa, J. Appl. Physiol. 105 (12) (2009) 124914.
[4] A. Kumar, D. Singh, R. Kumar, D. Kaur, J. Alloys Compd. 479 (2009) 166.
[5] J. Pelleg, L.Z. Zevin, S. Lungo, N. Croitoru, Thin Solid Films 197 (1991) 117.

[6] J.P. Zhao, X. Wang, Z.Y. Chen, S.Q. Yang, T.S. Shi, X.H. Liu, J. Phys. D: Appl. Phys. 30 (1997) 5.
[7] U.C. Oh, J.H. Je, J. Appl. Phys. 74 (1993) 1692.
[8] S.H.N. Lim, D.G. McCulloch, M.M.M. Bilek, D.R. McKenzie, J. Appl. Phys. 93 (2003) 4283.
[9] R. Banerjee, R. Chandra, P. Ayyub, Thin Solid Films 405 (2002) 64.
[10] T.Q. Li, S. Noda, Y. Tsuji, T. Ohsawa, H. Komiyama, J. Vac. Sci. Technol. A 20 (2002) 583.
[11] P. Patsalas, C. Gravalidis, S. Logothetidis, J. Appl. Phys. 96 (2004) 6234.
[12] S. Mahieu, P. Ghekiere, G. De Winter, S. Heirwegh, D. Delpha, R. De Gryse, O.I. Lebedev, G. Van Tendeloo, J. Cryst. Growth 279 (2005) 100.
[13] J.H. Je, D.Y. Noh, H.K. Kim, K.S. Liang, J. Appl. Phys. 81 (1997) 6126.
[14] Y. Cheng, Y.F. Zheng, IEEE Trans. Plasma Sci. 34 (4) (2006) 1105.
[15] M. Birkholz, K.-E. Ehwald, D. Wolansky, I. Costina, C. Baristiran-Kaynak, M. Fröhlich, H. Beyer, A. Kapp, F. Lisdat, Surf. Coat. Technol. 204 (2010) 2055.
[16] X. Liu, P.K. Chu, C. Ding, Mater. Sci. Eng. R: Rep. 47 (2004) 49.
[17] W.C. Oliver, G.M. Pharr, J. Mater. Res. 7 (1992) 1564.
[18] X.-J. Chen, V.V. Struzhkin, Z. Wu, M. Somayazulu, J. Qian, S. Kung, A.N. Christensen, Y. Zhao, R.E. Cohen, H.-k. Mao, R.J. Hemley, Proc. Natl. Acad. Sci. U. S. A. 102 (9) (2005) 3198.
[19] Inorganic crystal structure database (ICSD), http://icsd.fiz-karlsruhe.de/.
[20] G.B. Harris, Philos. Mag. 43 (1952) 113.
[21] C.S. Barrett, T.B. Massalski, Structure of Metals, Pergamon, Oxford, 1980, p. 204.
[22] J.H. Huang, K.-H. Chang, G.-P. Yu, Surf. Coat. Technol. 201 (2007) 6404.
[23] T.M. Muzyczko, Ind. Eng. Chem. Prod. Res. Dev. 17 (1978) 169.
[24] B. O'Brien, W.M. Carroll, M.J. Kelly, Biomaterials 23 (2002) 1739.
[25] D. Roman, J. Bernardi, C.L.G. de Amorim, F.S. de Souza, A. Spinelli, C. Giacomelli, C.A. Figueroa, I.J.R. Baumvol, R.L.O. Basso, Mater. Chem. Phys. 130 (2011) 147.
[26] G. Abadias, Surf. Coat. Technol. 202 (2008) 2223.
[27] J.L. Ruan, D.F. Lii, J.S. Chen, J.L. Huang, Ceram. Int. 35 (2009) 1999.
[28] R.L.O. Basso, R. Candal, C. Figueroa, D. Wisnivesky, F. Alvarez, Surf. Coat. Technol. 203 (2009) 1293.
[29] H. Park, J.A. Szpunar, Corros. Sci. 40 (4–5) (1998) 525.
[30] E. Portolan, C.L.G. Amorim, G.V. Soares, C. Aguzzoli, C.A. Perottoni, I.J.R. Baumvol, C.A. Figueroa, Thin Solid Films 517 (2009) 6493.
[31] D.F. Shriver, P.W. Atkins, C.H. Langford, Inorganic Chemistry, 2nd edition, Oxford University Press, Oxford, 1996, p. 302.
[32] C.A. Figueroa, F. Alvarez, D.R.G. Mitchell, G.A. Collins, K.T. Short, J. Vac. Sci. Technol. A 24 (2006) 1795.
[33] A. Leyland, A. Matthews, Wear 246 (2000) 1.